Geochimica et Cosmochimica Acta, Vol. 69, No. 9, pp. 2385–2398, 2005

0016-7037/05 $30.00 + .00

doi:10.1016/j.gca.2004.09.025

Rare earth diffusion kinetics in garnet: Experimental studies and applications

Massimiliano Tirone,[1,†] Jibamitra Ganguly,[2,*] Ralf Dohmen,[3] Falko Langenhorst,[4] Richard Hervig,[5] and Hans-Werner Becker[6]

[1]CeSMEC, Center for the Study of Matter at Extreme Conditions University Park Campus, Florida International University, Miami, Florida 33199 USA
[2]Department of Geosciences, University of Arizona, Tucson, Arizona 85721 USA
[3]Institut für Geologie, Mineralogie und Geophysik, Ruhr-Universität Bochum, D-44780, Bochum, Germany
[4]Bayerisches Geoinstitut, Universität, D-95440, Bayreuth, Germany
[5]Department of Geological Sciences, Arizona State University, Tempe, Arizona 85287 USA
[6]Institut für Physik mit Ionenstrahlen, Ruhr-Universität Bochum, 44780 Bochum, Germany

(*Received April* 7, 2004; *accepted in revised form September* 27, 2004)

Abstract—We determined the diffusion coefficient of Sm in almandine garnet as function of temperature at 1 bar and fO_2 corresponding to that of wüstite-iron buffer, and to a limited extent, that of a few other selected rare earth elements in almandine and pyrope garnets. Both garnets were demonstrated to have metastably survived the diffusion annealing at conditions beyond their stability fields. The experimental diffusion profiles were analyzed by secondary ion mass spectrometry, and in addition, by Rutherford back scattering spectroscopy for two samples. Transmission electron microscopic study of an almandine crystal that was diffusion-annealed did not reveal any near-surface fast diffusion path. Using reasonable approximations and theoretical analysis of vacancy diffusion, the experimental data were used to develop an expression of rare earth element (REE) diffusion coefficient in garnet as a function of temperature, pressure, fO_2, ionic radius, and matrix composition. Calculation of the closure temperature for the Sm-Nd decay system in almandine garnet in a metamorphic terrain shows very good agreement with that constrained independently. Modeling of the REE evolution in melt and residual garnet suggests that for dry melting condition, the REE pattern in the melt should commonly conform closely to that expected for equilibrium melting. However, for much lower solidus temperatures that would prevail in the presence of a H_2O-CO_2 fluid, the concentration of light REE in the melt could be significantly lower than that under equilibrium melting condition. A reported core and rim differences in the REE content of a garnet crystal in a mantle xenolith in kimberlite have been reproduced by assuming that the REE zoning was a consequence of entrapment in a magma derived from an external source for ~32,000 yr before the eruption. *Copyright © 2005 Elsevier Ltd*

1. INTRODUCTION

Rare earth element (REE) fractionation provides important constraints on the modeling of magmatic and metamorphic processes. In mantle rocks, which undergo partial melting, garnet and clinopyroxene are the major hosts of the REE. These minerals are also major hosts of REE in metamorphic rocks. Thus, there is considerable interest in the study of the thermodynamic and diffusion kinetic behavior of REE in garnet and clinopyroxene that could help to understand the evolution of REE patterns in magmas and in the residual solids, and also the REE zoning in these minerals, especially garnets, in igneous and metamorphic rocks. In addition, it is important to have reliable data on the diffusion kinetic properties of Sm and Nd in garnet for the proper interpretation of the Sm-Nd mineral ages in relation to the peak metamorphic conditions and cooling rates (e.g., Ganguly et al., 1998; Ducea et al., 2003).

Local equilibrium, that is, equilibrium over defined spatial and time scales between coexisting minerals and fluid or melt, have usually been assumed in the theoretical models of REE evolution in melts. While equilibrium was most likely achieved at the mineral-melt interface during partial melting, the slow diffusivity of a component in a mineral could lead to the development of compositional gradient, the extent and nature of which depend on the thermal history and magma residence time. The fractionation of a component between a mineral and melt not only depends on their equilibrium distribution coefficient, but also on the diffusion properties of the component in the mineral. Thus, a so-called "incompatible" element, which fractionates into a melt in preference to a solid, may show an *effectively* "compatible" or less incompatible behavior because of its slow diffusivity in the mineral in relation to the residence time of the magma.

Ganguly et al. (1998) determined the Sm and Nd diffusion kinetics in almandine garnet ($Alm_{77}Prp_{22}Gr_3$) at 1 bar, 777 to 877°C with fO_2 defined to that of wüstite-iron (WI) buffer by means of a flowing mixture of CO and CO_2. They found no significant difference between the diffusivities of these two rare earth elements in almandine. Recently, Van Orman et al. (2002a) determined the diffusion kinetics of the rare earth elements Ce, Sm, Dy, and Yb in a pyrope garnet ($Alm_{16}Pyr_{71}Gr_{13}$) at 28 kb, 1200 to 1400°C in a piston-cylinder apparatus with the fO_2 buffered by graphite and the prevailing C-O fluid under nominally anhydrous condition. The diffusion profiles were analyzed by depth profiling in an ion probe by secondary ion mass spectrometry (SIMS), as in the earlier study by Ganguly et al. (1998). Comparison between the data of Van Orman et al. (2002a) and Ganguly et al. (1998) requires substantial extrapolation in the P-T-fO_2-X space, where X stands

* Author to whom correspondence should be addressed (ganguly@geo.arizona.edu).
† Present address: Department of Earth & Atmospheric Sciences, Cornell University, Ithaca, New York 14853-1504 USA

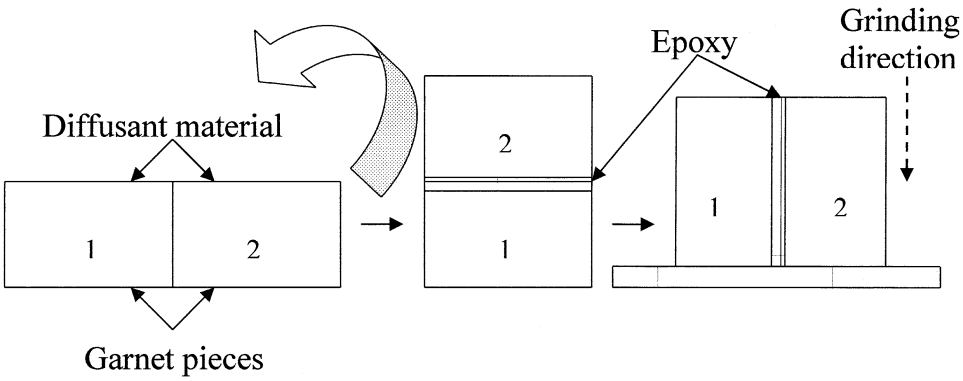

Fig. 1. Preparation of garnet sample for TEM study. A garnet single crystal was cut into two pieces, 1 and 2 (left panel). The top surfaces of the two pieces containing the diffusant material were glued together by epoxy (central panel), and then set on a glass slide (right panel). The assembly of the two garnet pieces was ground down from the top, as shown by the dashed arrow to 30 μm thickness.

for composition. Adequate data for such extrapolation are not available at present. However, ignoring compositional dependence of the tracer diffusion of REE in garnet and assuming an activation volume, ΔV^+, of 10 cm^3/mol, Van Orman et al. (2002a) noted that their Sm diffusion data in garnet are about an order of magnitude smaller than those of Ganguly et al. (1998) at the same P-T conditions (a more detailed comparison between these two data sets will be presented later this paper). The assumption about ΔV^+ by Van Orman et al. (2002a) was based on a survey of the available data ΔV^+ for divalent cations in garnet.

The disagreement between the extrapolated data of Van Orman et al. (2002a) and Ganguly et al. (1998) prompted us to reexamine the samples in the latter study to see if somehow these have yielded larger values of diffusion coefficients due to the presence of near-surface defects and analytical artifacts. For this purpose, we studied selected samples from Ganguly et al. (1998) by transmission electron microscopy (TEM) and by Rutherford backscattering spectroscopy (RBS). In addition, we determined the tracer diffusion coefficients of Nd in pyrope garnet ($Alm_{38}Prp_{50}Gr_{12}$) to check if there is any significant compositional dependence of the tracer diffusivities of the REE in garnet that might have contributed to the apparent difference between the results of Ganguly et al. (1998) and Van Orman et al. (2002a). The latter workers showed that, unlike clinopyroxene (Van Orman et al., 2001), there is no significant influence of ionic radius on the tracer diffusivities of REE in garnet. This is consistent with the preliminary results reported by Tirone et al. (2000). We also report in this paper the results of tracer diffusion experiments of Nd (1.12 Å), Sm (1.09 Å), Gd (1.06 Å), and Yb (0.98 Å) in garnet, where the parenthetical numbers are ionic radii in the eight coordinated site (Shannon and Prewitt, 1969), to evaluate the influence of ionic radii on the tracer diffusivites of REE in garnet. In addition, we discuss some applications of the data on REE diffusivities in garnet to geological problems.

2. TRANSMISSION ELECTRON MICROSCOPIC STUDY OF GARNET

2.1. Sample and Method

An almandine garnet sample ($Alm_{75}Pyr_{22}Gr_3$) that was annealed by Ganguly et al. (1998) for 159 h at 1 bar, 777°C (experiment Gt 10) was selected for TEM studies. This is one of two almandine samples that were annealed simultaneously. Although the experimental conditions were outside the stability of garnet of above composition (Hsu and Burnham, 1969), the metastable survival of garnet was initially checked by X-ray diffraction of garnet powder that was annealed at 900°C at fO_2 of WI buffer for 42 h. The fO_2 of the diffusion experiment was controlled to that of WI buffer by a mixture of CO and CO_2 that flowed through a vertical tube furnace at controlled rates. The details of the sample preparation technique are given in Ganguly et al. (1998). The sample was cut into two pieces normal to the surface on which the diffusant material was deposited. These pieces were glued back together on the surfaces containing the diffusant material and mounted with a thermal glue on a glass slide that was placed normal to the mating plane (Fig. 1). The sample was then polished down to a 30 μm thin section parallel to the glass plate. A 3 mm wide copper grid was glued with epoxy resin on to the polished surface. The thin section, including the mounted copper grid, was removed from the glass slide by dissolving the thermal glue with acetone. Subsequently, the sample was thinned by argon ion bombardment at 4.5 keV accelerating voltage and 1 mA beam current at an angle of incidence of 14°. A thin strip of epoxy was drawn at the interface of the two garnet pieces to prevent it from preferential thinning during ion milling. Electron microscopic observation was then carried out with a Philips CM20 field emission gun (FEG) TEM operating at 200 kV.

2.2. Results

Figure 2a shows a bright-field image of the garnet just below the surface on which the diffusant material was deposited. The upper part of the picture shows the epoxy resin that was used to glue the two cut pieces together, as described above. The garnet is found to be essentially free of linear and planar lattice defects. Figure 2b shows a high-resolution TEM image along the [111] zone axis of a portion of the garnet crystal that is located ~50 nm from the surface. It shows nothing other than perfectly ordered garnet that is free of any linear or planar defects. These pictures are representative of our observations in three different places of the garnet, where it was transparent to a depth of 10 μm from the original surface. Thus, the TEM

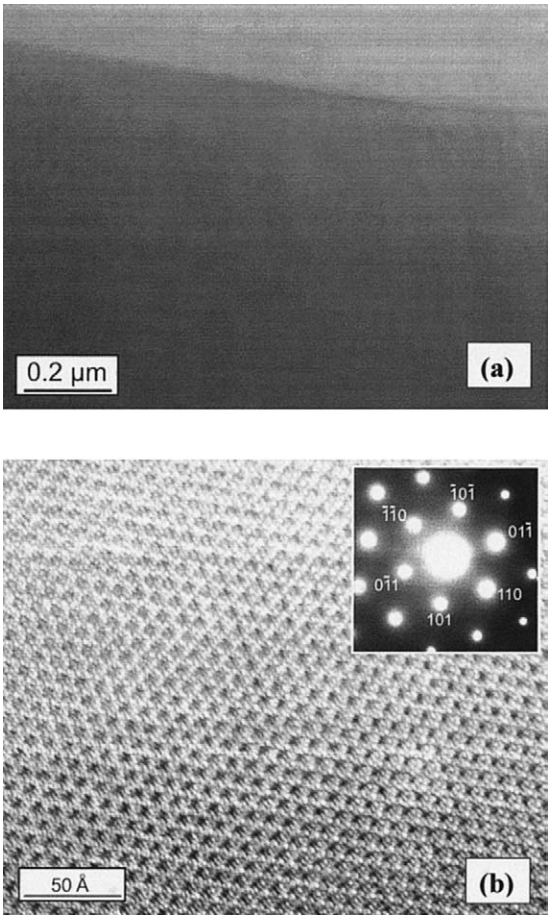

Fig. 2. (a) Bright-field TEM image of garnet just below the surface on which the diffusant material was deposited. The upper part (lighter part) of the picture shows the epoxy resin that was used to glue the two cut pieces together. (b) High-resolution TEM image along the [111] zone axis of a portion of the garnet crystal that is located ~50 nm from the surface.

study does not show any fast diffusion path near the surface, or breakdown of garnet to other phases, despite annealing outside its field of stability that could have affected the diffusion data.

3. RUTHERFORD BACK SCATTERING SPECTROSCOPY

Rutherford back scattering spectroscopy (RBS) is an energy spectroscopy that can be interpreted as a depth resolved mass spectrometry of near-surface layers (depth <1 μm). The general principles, along with mineralogical applications, have been reviewed by Jaoul et al. (1991). Using the RBS facility at the Dynamitron Tandem accelerator at the Ruhr University, Bochum, we analyzed two samples, Gt5 and Gt6r, from the set of samples that were already analyzed by Ganguly et al. (1998) by SIMS (Table 1). The experimental conditions of these samples were 777 and 877°C, respectively, with the pressure at 1 bar and fO_2 corresponding to that of WI buffer.

3.1. Measurement and Fitting of RBS Spectra

For the SIMS analyses, a sample surface with the diffusant material was coated with a thin film of gold to prevent charge buildup. However, since gold has a strong signal near that of REE in the RBS spectrum (which cannot resolve the signals from the different REE), it was necessary to remove the Au coating from the sample surface before RBS analysis, but without damaging the sample surface. Following Ryerson and McKeegan (1994), we tried to remove the Au coating by sonicating the sample in an aqueous solution of KI. Although KI solution removed significant amount of the Au coating, the latter was never dissolved out completely, even after a few hours of sonication in KI bath in fresh batch of concentrated KI solution. We tried to find sufficiently large Au-free surface areas in the samples that could be analyzed by RBS without significant interference from Au signal.

The RBS analyses were carried out using a 20 nA, 2 MeV beam of $^4He^+$ (alpha) particles. The integrated charge of the alpha particles in a measurement was within 120000 and 180000 nC. The beam was collimated to a diameter of 0.5 mm and was used in combination with a silicon particle detector at a backscattering angle of 170°. The resolution of the energy detector was 16 keV. The depth resolution of RBS analysis is given by the product of detector resolution and stopping power of alpha particles. For the composition and density of the garnet samples, the latter was estimated to be ~ 0.4 keV/nm. Thus, the depth resolution was estimated to be ~ 6 nm.

The RBS spectra were simulated using the software RBX (Kotai, 1994) that permits the user to vary the sample composition as a function of depth. The fitting of the RBS spectra was performed through several iterations. Initially a spectrum was calculated on the basis of the microprobe analysis of the sample, and compared with the measured spectrum. The difference between the two spectra was then minimized by introducing depth variation of composition. Because of the overlap of the signals for Nd and Sm in the RBS spectra, both Sm and Nd were treated as a single species. This does not introduce any serious error since these rare earths have very similar diffusivities (Ganguly et al., 1998; Van Orman et al., 2002a). The accuracy with which the content of a specific element in a solid could be determined depends on its concentration level, atomic number, the counting statistics, and chemical composition of the matrix.

For the simulation of the RBS spectra of the samples Gt5 and Gt6r, it was necessary to introduce three different zones from the surface towards the interior of the crystal: (1) a very thin zone, ~20 and 30 nm thick, containing the residual layer, (2) a diffusion zone with a gradual change of the composition, and (3) the host crystal unaffected by REE diffusion. Figure 3a shows the RBS spectrum of the sample Gt 5 and its simulated fit. It is found that except for the first 100 nm from the surface, which also includes the residual layer of the diffusant material, the measured spectrum can be simulated almost exactly by the one calculated on the basis of the microprobe analysis of the garnet sample. To fit the RBS data for the first 100 nm, the following variation in the content of Ca, Fe, and Al, on 12 oxygen basis per formula unit, had to be made from their respective bulk values: (a) smooth increase of Ca from 0.09 bulk value in the garnet to 0.45 toward the surface within the first 30 nm; (b) smooth decrease of Fe from 2.25 (bulk value) to 2.02, and of Al from 2.0 (bulk value) to 1.9 toward the surface within the first 100 nm. For the sample Gt6r, the diffusion zone is ~200 nm deep, and compared to Gt5, the

Table 1. Summary of experimental conditions and retrieved diffusion coefficients, D, of Sm, Nd, Gd, and Yb in garnet. Gt: $Alm_{75}Pyr_{22}Gr_3$; Py: $Alm_{38}Pyr_{50}Gr_{12}$. All experiments are at 1 bar and fO_2 corresponding to that of wüstite-iron buffer. D values are in cm^2/s. The parenthetical numbers are $\pm$ 1σ, preceded by a decimal point, resulting from the scatter of the data measured by depth profiling in an ion-probe. All experiments, except those indicated by asterisks (**), were used in Ganguly et al. (1998).

Run No	T (°C)	Time (hr)	logD(Nd)	logD(Sm)	logD(Gd)	logD(Yb)
Gt 5b-1	777	159.15	−16.88 (05)	−16.85 (05)		
Gt 5b-2	777	159.15	−16.89 (05)	−16.79 (06)		
Gt 10-1	777	159.15	−16.82 (07)	−16.80 (06)		
Gt 10-2	777	159.15	−16.83 (07)	−16.78 (06)		
Gt 10-3	777	159.15	−16.78 (07)	−16.76 (07)		
Py 3**	777	151.00	−17.11 (06)		−17.03 (09)	−16.97 (10)
Gt 22	800	8.00	−16.52 (08)	−16.45 (07)		
Gt 3-2	827	72.00	−16.25 (06)	−16.22 (03)		
Gt 3-3	827	72.00	−16.37 (04)			
Gt 4-1	827	72.00	16.07 (08)	−16.04 (07)		
Gt 4-2	827	72.00	−16.10 (05)	−16.07 (06)		
Gt 4n-1	827	72.00	−16.35 (03)	−16.34 (03)		
Gt 4n-2	827	72.00	−16.14 (02)			
Gt 4n-3	827	72.00	−16.41 (03)	−16.40 (03)		
Gt 6r	877	41.50	−16.00 (02)	−15.96 (02)		
Gt 9r-1	877	18.25	−15.90 (07)	−15.89 (06)		
Gt 9r-2	877	18.25	−15.88 (05)	−15.84 (04)		
Gt 11	877	18.25	−15.96 (04)	−15.90 (05)		
Gt 11r	877	18.25	−15.96 (03)	−15.90 (04)		
Gt 16V	877	76.00	−15.66 (08)	−15.60 (11)		
Gt 13-1**	877	19.00			−15.54 ((01)	−15.39 (03)
Gt 13-2**	877	19.00			−15.65 (01)	−15.54 (02)
Gt 15**	877	46.00			−15.83 ((03)	−15.81 (02)
Py 1**	900	63.15	−16.11 (04)		−16.00 (01)	−15.90 (06)
Gt 20b**	927	43.40			−15.27 (04)	−15.26 (05)

concentration of REE and the corresponding changes for Fe and Al are larger.

The inset in Figure 3a shows that there is no significant overlap from other elements with the Sm + Nd signal, at least within 1700 to 1800 keV energy range. The concentration vs. depth profile of Sm + Nd for the sample Gt5 is shown in Figure 3b. The concentration is essentially flat up to $\sim$ 20 nm from the surface, followed by a monotonic decrease reaching a plateau value at $\sim$ 90 nm. We interpret the data in the first 20 nm as the homogeneous composition within the residual diffusant layer on the garnet surface.

3.2. Retrieval of Diffusion Coefficient and Discussion

Since RBS can not distinguish among different rare earth elements, both Sm and Nd that were codiffused into the chosen garnet samples were treated as a single species. Assuming constant diffusion coefficient, D, and that the diffusant layer acted as a homogeneous infinite reservoir; the solution to the one-dimensional diffusion in a semi-infinite medium is given by Crank (1975), Eqn. 2.45. Modeling of the RBS data according to this relation yields $D = 4.5 \times 10^{-18}$ cm^2/s for Gt5 (Fig. 3b) and $D = 8.5 \times 10^{-17}$ cm^2/s for Gt6r.

We have also modeled the diffusion data assuming a homogeneous film of finite reservoir of the diffusant material on the crystal surface. Assuming (a) different but constant diffusivities within the film and semi-infinite crystal substrate, (b) the initial concentration of the diffusing species in the crystal to be effectively zero, and (c) the flux at the surface of the film to be zero, the appropriate solution of the diffusion equation was derived by Lovering (1938). Modeling of the RBS data according to this solution yields essentially the same D values for the two garnet samples as those obtained from assuming semi-infinite reservoir.

The uncertainty in the retrieved values of the diffusion coefficients derive from the errors in the estimation of the thickness of residual layer, depth resolution and background correction of the RBS spectrum, and fitting of the concentration vs. depth data. We estimated the error in the diffusion coefficient retrieved from each RBS spectrum by varying the thickness of the residual layer and background correction for the simulation of the spectra and fitting the resulting diffusion profiles. From this exercise, we obtained errors of logD values to be $\sim$ 0.5 for the sample Gt1 and $\sim$0.1 for the sample Gt6r. It is difficult to exactly characterize these error estimates in terms of statistical standard deviations (σ), but these represent a high degree of confidence interval, perhaps approximating that of 2σ, for the estimated values of logD. The significantly smaller error for the sample Gt6r is due to the longer profile length ($\sim$150 nm), which leads to smaller effect of the error in depth resolution and the residual layer thickness on the profile fitting.

The near-surface enrichment of Ca in the RBS spectrum seems to be almost entirely confined within the residual diffusant film and is likely to be a result of contamination. The depletion of Al in the RBS data near the surface of the garnet crystals is likely to be related, at least in part, to the mechanism of Nd incorporation in garnet. Tirone (2002) carried out molecular dynamic simulation of the Nd diffusion kinetics in garnet based on assumed mechanisms of defect formation and Nd^{3+} incorporation in garnet. He considered a few alternative mechanisms for defect formation and Nd^{3+} incorporation in

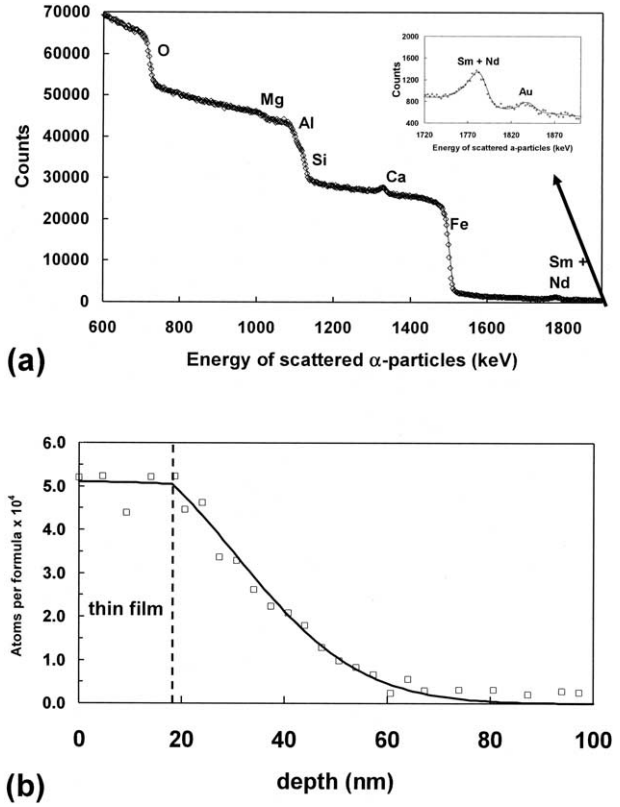

Fig. 3. (a) RBS spectra of the sample Gt5, along with characteristic energy edges of the elements, and the simulation of the spectra. Note the small peaks at ~ 1340 keV and 1790 keV due to enrichment of Ca and Sm/Nd (see inset), respectively, and the small gradient between energy 1400 keV and 1500 keV due to loss of Fe. (b) Concentration vs. distance plot for Sm plus Nd and model fit (solid line) that yields D = $4.5(10^{-18})$ cm^2/s. The dotted line at a depth of 20 nm indicates the estimated thickness of a residual layer of the rare earths on the crystal surface.

the garnet structure, and the combination that produced Nd^{3+} diffusion kinetics in agreement with the experimental data of Ganguly et al. (1998) required progressive depletion of Al toward the surface within the diffusion zone. However, the extent of depletion that is suggested by the RBS spectrum seems to be somewhat in excess of what is needed for Nd^{3+} diffusion in garnet. The near-surface depletion of Fe in the RBS spectrum remains unexplained.

4. DEPENDENCE OF DIFFUSION COEFFICIENT ON GARNET COMPOSITION AND REE RADIUS

4.1. Experimental Procedure and Metastability of Garnets

We have carried out limited experiments using Mg-rich garnet, $Al_{38}Prp_{50}Gr_{11}Sps_1$, and Fe-rich garnet, $Alm_{75}Pyr_{22}Gr_3$, at a pressure of 1 bar and fO_2 corresponding to those of WI buffer to roughly estimate the effects of garnet composition and ionic radii on the diffusion coefficients of REE. The preparation of rare earth isotope enriched dilute HCl solution and the experimental procedure are the same as described by Ganguly et al. (1998). Briefly, the solutions of metals enriched in ^{152}Sm, ^{158}Gd, and ^{174}Yb were prepared by first dissolving the metals in 2N HCl solution, evaporating it to almost complete dryness, and then adding triple-distilled water so that there was 100 to 200 ppm of the enriched isotopes in the solution, as determined by an inductively coupled mass spectrometer (ICP-MS). The samples were polished on one side to mirror finish by a combination of mechanical and chemical polishing, and all samples were preannealed at, or close to, the experimental conditions to enable equilibration of the point defects and to heal any fast diffusion paths. Drops of all three solutions were deposited onto polished sample surfaces of almandine- and pyrope-rich garnets. Two experiments were also performed with Fe-rich garnet with only codeposited solutions of ^{158}Gd and ^{174}Yb. After diffusion anneal at the desired conditions, the samples were quenched and analyzed by depth profiling in a Cameca ims 3f SIMS using a primary beam of mass filtered $^{16}O^-$ accelerated to 10 keV. Further details about the analytical protocol can be found in Ganguly et al. (1998).

The evidence for the metastable survival of almandine crystals has been discussed in the section 2.1 dealing with transmission electron microscopy. No TEM study was, however, carried out on the Mg-rich garnet. We checked for the metastable survival for this garnet at the highest temperature of our experiments, 900°C, at 1 bar and fO_2 corresponding to that of WI buffer, in two ways: (a) A powdered sample of Mg-rich garnet was annealed at this condition for 43 h and X-rayed to check for the breakdown of garnet. No new phase was detected in the X-ray diffraction pattern. (b) One side of the sample Py1 (Table 1), which was diffusion-annealed at the above condition for 63 h (Table 1), was polished and carefully examined in an electron microprobe using SEM, BSE, and X-ray images to find

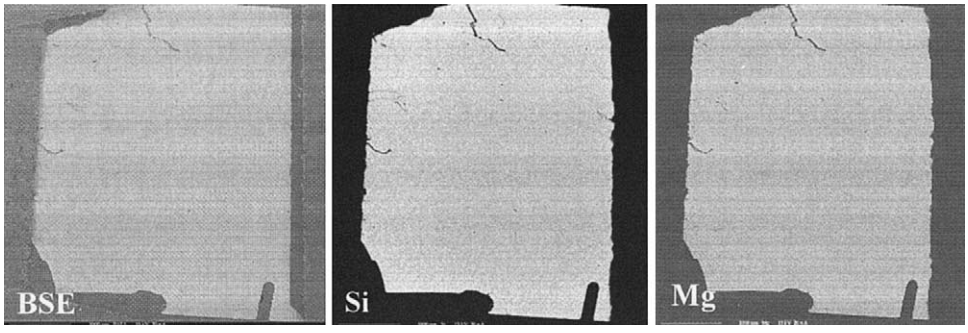

Fig. 4. Backscattered electron image (BSE) and Mg and Si X-ray maps of a side of the garnet crystal Py1 that was diffusion-annealed at 1 bar, 900°C, fO_2 corresponding to that of WI buffer for 63 h (Table 1). The sample is ~ 4.5 mm across.

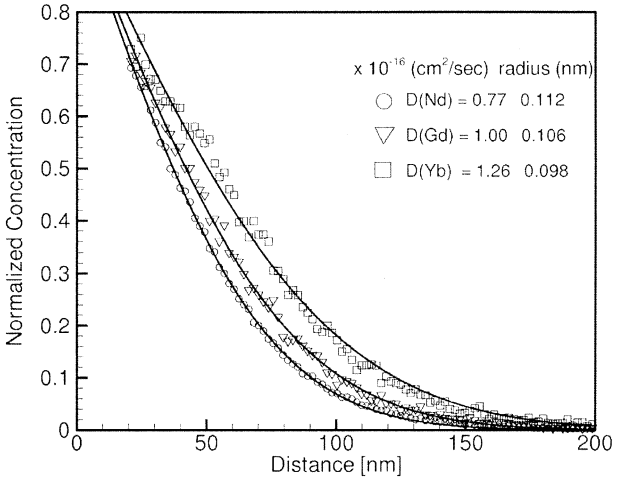

Fig. 5. SIMS depth profiling data for Nd, Gd, and Yb in a pyrope garnet, $Al_{38}Prp_{50}Gr_{12}$, and the fitted diffusion profiles. The experimental conditions were 1 bar, 900°C at fO_2 corresponding to that of WI buffer. There are no data in the first 200 Å because of instability of the analysis within this range, which is typical for SIMS analysis.

any evidence of decomposition. The BSE image and X-ray maps for Mg and Si are shown in Figure 4. The images are completely monotonous and, thus, do not show any evidence of decomposition of the Mg-rich garnet. In addition, a total of 112 spot analyses were taken in different parts of the sample. The results show exceptionally uniform composition with garnet stoichiometry in which the variations of atomic fractions of Fe, Mg, Ca, and Mn are within 0.01.

4.2. Modeling and Results

The experimental data were modeled using solutions of the one-dimensional diffusion equation for both semi-infinite reservoir and depleting source (Crank, 1975), interfacing the solutions with an optimization program. However, as in Ganguly et al. (1998), the solution for the first condition yielded better fit to the diffusion data. Figure 5 shows an example of the experimental and fitted tracer diffusion profiles of Nd, Gd, and Yb in garnet. The experimental conditions and the retrieved REE diffusion data in both almandine and pyrope rich garnet, along with those from the earlier study by Ganguly et al. (1998), are summarized in Table 1. The details of the diffusion data were not published in the latter study due to space limitation. Some of these data are slightly different from those in Ganguly et al. (1998) as a result of further refinement of the modeling procedure.

The errors in the diffusion coefficients summarized in Table 1 are those arising from the scatter of the C vs. X data. The standard deviations were calculated numerically: for a given data set, the best fit diffusion coefficient, D, was given a certain error (eD), and the number of data points that were included within the range of profiles defined by D ± eD was counted by a computer. Assuming that the fraction of the included data represents the fractional area under the Gaussian distribution function, the assigned error value was converted to a multiple of standard deviation (σ) from the table of integrals for the Gaussian function. For example, if 80% data points of a measured profile were included within the range of profiles calculated according to D ± eD, then the assigned error eD equals 1.3σ. In terms of the percentage of the D values, the average values of standard deviations of the D(Nd), D(Sm), D(Yb), and D(Gd) obtained according to this procedure are $\sigma_{D(Nd)} \approx \sigma_{D(Sm)} \approx 11\%$, and $\sigma_{D(Yb)} \approx \sigma_{D(Gd)} \approx 7\%$.

In addition to the above error, there are also errors in D arising from those in the measurement of crater depth. Several measurements of a few selected crater depths indicate a total variation of ~ ± 5%. If we take that to define the 95% confidence interval, then the standard error in the measurement of the crater depth may be taken as ~ 2.5% of the measured depth. Since D α x^2, where x is the length of a diffusion profile, 2.5% change in the value of x translates to a change of D by 5%.

Two important observations can be made from the diffusion data summarized in Table 1:

(a) The Nd diffusion value in the pyrope-rich garnet at 777°C is 0.3 log unit smaller than that in almandine garnet, whereas at 900°C, it is 0.6 log unit smaller than that interpolated from the Arrhenian relation (see below) for the almandine garnet. Thus, a change of garnet composition from $Alm_{75}Pyr_{22}Gr_3$ to $Alm_{38}Pyr_{50}Gr_{12}$ seems to have caused a reduction of the logD(Nd) value by ~ 0.5, which is equivalent to a reduction of D by a factor of ~ 3. This effect is probably due to a decrease of cell volume of garnet and/or decrease of vacancy concentration, which is related to the Fe^{2+} according to $3Fe^{2+} + 1/2O_2 \rightarrow 2Fe^{3+}$ + [cation vacancy] + FeO. Extrapolating this effect, it seems possible that changing the garnet composition from the one

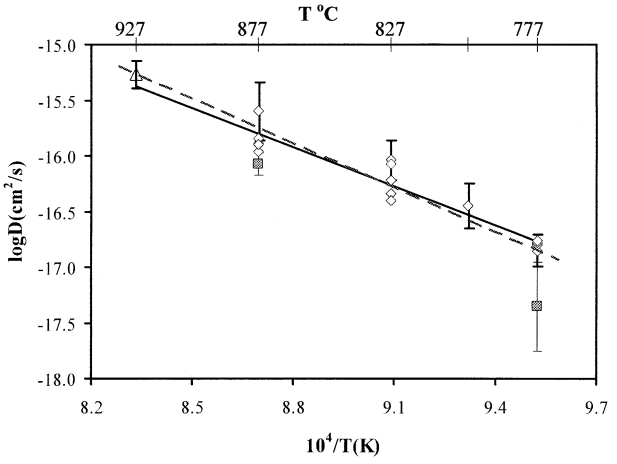

Fig. 6. Arrehenian relation of the diffusion coefficient of Sm (diamonds) in almandine ($Alm_{75}Pyr_{22}$) garnet, along with the diffusion coefficient of Gd at 927°C (triangle), at 1 bar and fO_2 corresponding to that defined by WI buffer. All open symbols represent diffusion coefficient retrieved from the SIMS data. The filled squares are diffusion coefficients retrieved from RBS data. The solid line is the unweighted least squares fit to the SIMS data, while the dashed line is a preferred fit with the maximum activation energy permitted by the data. The error bars on selected SIMS data indicate approximately $\pm 2\sigma$ estimates (95% confidence interval) of the individual D values considering the scatter of the compositional data and error in the measurement of crater depth, while those on the RBS data represent probable estimates of similar confidence interval (see text).

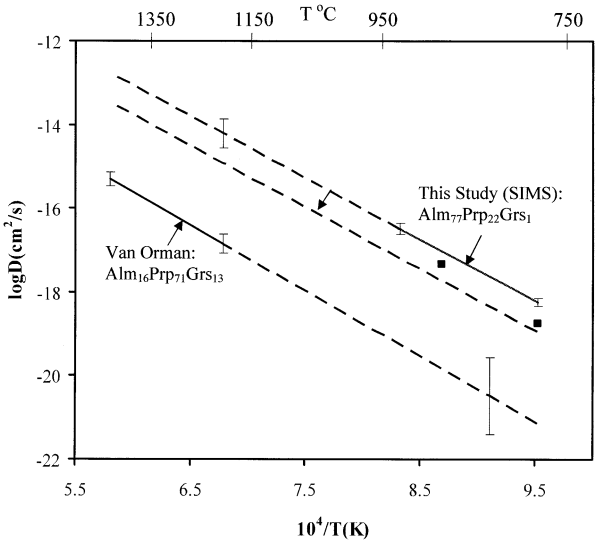

Fig. 7. Comparison of the Sm diffusion data obtained from SIMS analyses of diffusion profiles in this study, normalized to P = 28 kb, with those of Van Orman et al. (2002a) determined experimentally at the same pressure. All data are normalized to fO_2 corresponding to that defined by WI buffer (see text). The solid lines represent the range of experimental temperatures in both studies. The error bars indicate the 95% confidence interval ($\pm 2\sigma$) of the estimated logD values from the regressed parameters (Eqn. 2). The filled squares represent the RBS data obtained in this study (see Fig. 6). The dashed line with arrow indicates the possible shift of our data due to the change of garnet composition from $Alm_{75}Prp_{22}Grs_1$, which was used by us, to $Alm_{16}Prp_{71}Grs_{13}$ that was used by Van Orman et al. (2002a).

used by Ganguly et al. (1998), $Alm_{75}Pyr_{22}Gr_3$, to that used by Van Orman et al. (2002a), $Alm_{16}Pyr_{71}Gr_{13}$, could cause a reduction of D(Nd) by a factor ~ 7. In extrapolating the effect of Mg content on D(Sm), we assumed that logD changes linearly with the atomic fraction of Mg, X_{Mg}. This assumption is based on the observation that in olivine logD(Fe-Mg) vs. X_{Mg} is essentially linear (Misener, 1974), where D(Fe-Mg) is the Fe-Mg interdiffusion coefficient. More work, however, is needed to develop a scheme of compositional effect on REE diffusion kinetics in garnet.

(b) Tracer diffusion kinetics of REE in garnet seem to have a weak dependence on the radius of the cation, which reinforces the conclusion of Van Orman et al. (2002a) and the preliminary finding of Tirone et al. (2000), but which is in contrast to the effect of ionic radius on the REE diffusion kinetics that was observed by Van Orman et al. (2001) in clinopyroxene. The diffusion profiles for Nd, Gd, and Yb in the pyrope garnet are illustrated in Figure 5.

5. ARRHENIAN TREATMENT AND COMPARISON OF SM DIFFUSION DATA

5.1. Diffusion Data from SIMS and RBS Analyses

Figure 6 illustrates the Sm diffusion data (diamonds) in almandine garnet that have been derived by modeling the diffusion profiles determined by SIMS. We do not have any data for Sm or Nd diffusion at the highest temperature of our experiments, which is 927°C. However, we have shown the SIMS-diffusion datum for Gd as a proxy for the Sm diffusion datum, since at this temperature there seems to be negligible effect of radius on the diffusion kinetics of rare earth elements in garnet (Table 1). The error bars on the SIMS data represent ~ $\pm 2\sigma$ values that include the errors arising from both C_i and x, as discussed above. Least squares fit to the Sm (+ Gd) diffusion data, giving equal weight to all data, yields ($\pm 1\sigma$)

$$\log D(Sm) = -6.0(\pm 0.7) - \frac{11735(\pm 775)}{T} cm^2/s, \quad (1a)$$

which corresponds to an activation energy, Q, of 224,681(± 14,836) J/mol. Since we only have a rough estimate of the effect of error in the measurement of crater depth on the diffusion coefficients, we did not feel that we could properly weight the diffusion data. As compared to the above value of Q(Sm), the diffusion of Mg and Fe^{2+} in garnet is associated with activation energies of 255 to 272 kJ/mol (Ganguly et al., 1998). On the basis of consideration of ionic charge and radius (IR), we argue that the activation energy of Sm^{3+} (IR(VIII) = 1.09 Å; Shannon and Prewitt, 1969) diffusion in garnet should be larger than that of the divalent cations, which have smaller ionic radii. Thus, we prefer a fit to the Sm diffusion data with the upper 2σ limit of activation energy, Q = 254353 J/mol. This procedure yields

$$\log D(Sm) = -4.2 - \frac{13285}{T}, cm^2/s \quad (1b)$$

(which can be recast in the standard Arrhenius form, D =

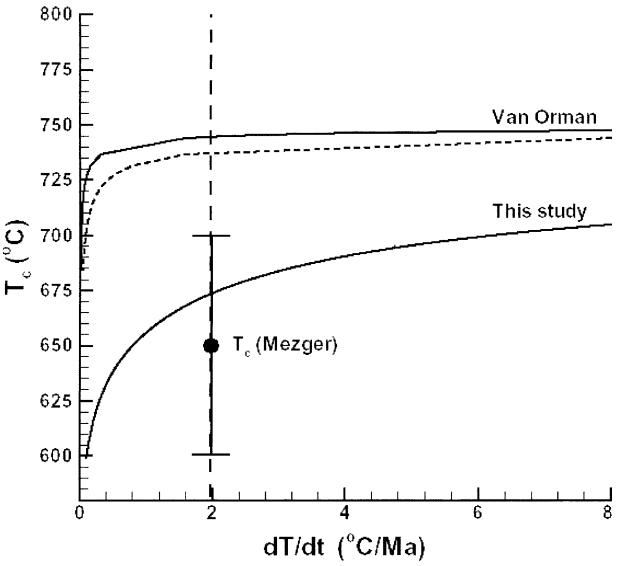

Fig. 8. Comparison of the closure temperature, T_c, of Sm-Nd decay system in an almandine garnet crystal of 1.5 mm radius using the diffusion data of this study and of Van Orman et al. (2002a) with the T_c estimated for a natural almandine garnet (filled circle with error bar) in the Pikwitonei Granulite Domain by Mezger et al. (1992). The latter estimated the initial P-T condition to be 8 kb, 750°C and a cooling rate of 2°C/Myr. The solid line for Van Orman indicates T_c vs. cooling rate without correction for the compositional effect, whereas the dashed line indicates that with correction for the compositional effect. The activation volume of diffusion, ΔV^+, is assumed to be 10 cm^3/mol. A smaller ΔV^+ improves the agreement of T_c (this study) with that of Mezger et al. (1992).

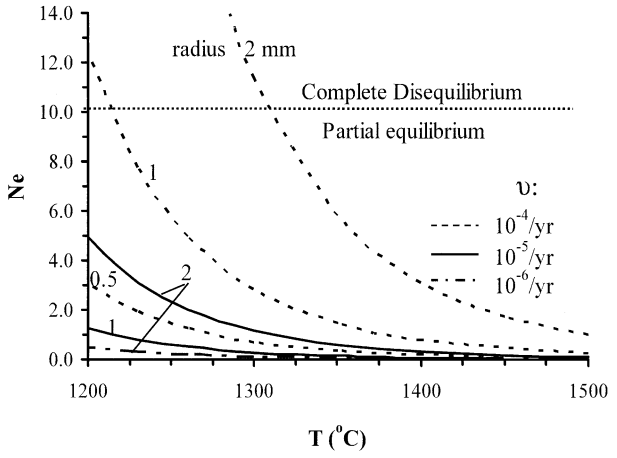

Fig. 9. Variation of disequilibrium parameter, Ne, with temperature for selected melting rates. Ne incorporates the effects of melting rate, grain size, and diffusion in solid on the dynamic melting behavior. It is defined as $\upsilon(R_o)^2/D$, where υ is the melting rate, normalized to the initial crystal volume, R_o is the initial crystal radius and D is the diffusion coefficient. For K (equilibrium distribution coefficient) <0.01, almost complete disequilibrium and equilibrium prevail for Ne >10, and Ne <0.1, respectively.

$D_o\exp(-Q/RT)$, with $D_o = 6.3 \times 10^{-5}$ cm^2/s). The expression of logD(Nd) is effectively the same, as should be evident from the D(Sm) and D(Nd) data in Table 1. The fitted relations, according to Eqn. 1a and 1b, are illustrated by solid and dashed lines, respectively, in Figure 6.

The composite diffusion coefficients of Sm and Nd of the sample Gt5 and Gt6r, as determined from the RBS data, are plotted in Figure 6 as filled squares. The error bars on the RBS data represent the total spread of the retrieved D values as discussed in section 3.3. There is good agreement between the SIMS and RBS data for the sample Gt6r, while there is a marginal agreement, considering the error limits, between the two types of data for the sample Gt5. Inclusion of the RBS data in the development of the Arrhenian relation for D(Sm) essentially yields the preferred fit, as given by Eqn. 2.

5.2. Comparison of Sm Diffusion Data and Synthesis

To compare our Sm diffusion data with those of Van Orman et al. (2002a), we need to normalize the two data sets to the same pressure, fO_2 condition, and garnet composition. For the purpose of comparison, we chose P = 28 kb, which is the pressure of the experimental data of Van Orman et al. (2002a), and fO_2 as that defined by the WI buffer at the P-T conditions. No data are yet available on the activation volume, ΔV^+, of REE diffusion in garnet that is needed to normalize the diffusion data to a chosen pressure. However, after reviewing the available data on divalent cation diffusion (Fe, Mg, Mn and Ca) in garnet, Van Orman et al. (2002a) assumed $\Delta V^+(Sm) \sim 10$ cm^3/mol, which is approximately the upper limit of the measured ΔV^+ values for the divalent cations. From the fO_2 values defined by graphite plus C-O fluid and WI buffer at high P-T conditions, as calculated by Chakraborty and Ganguly (1992), we conclude that the fO_2 condition defined by graphite in the experimental studies of Van Orman et al. (2002a) is ~ 6 orders of magnitude higher than that defined by the WI buffer at the same P-T conditions. The diffusion coefficient in garnet is assumed to vary as $(fO_2)^{1/6}$, which is the relation suggested by the theoretical analysis of the dependence of point defects in a ferromagnesian mineral on fO_2 (e.g., Morioka and Nagasawa, 1991). The fO_2 dependence of D could be somewhat different from this relation in specific cases (e.g., Nakamura and Schmalzreid, 1984; Petry et al., 2004).

Figure 7 shows a comparison of our Sm diffusion data with those of Van Orman et al. (2002a) at a pressure of 28 kb and fO_2 defined by the WI buffer, taking into consideration the effect due to the pressure dependence of the buffer, as discussed by Chakraborty and Ganguly (1992). The square symbols show the results obtained from the RBS analyses of the diffusion profiles of the samples Gt5 and Gt6r. Accounting for the potential effect of garnet composition, as deduced above, the D(Sm) may be lowered by ~ 0.9 log units to approximate its value in the pyrope-rich garnet composition, $Alm_{16}Pyr_{71}Gr_{13}$, that was used by Van Orman et el. (2002a). This estimated shift of D(Sm) is illustrated by a dashed line in Figure 7. The error bars represent $\pm 2\sigma$ values (95% confidence interval), which were calculated according to

$$\sigma_Y^2 = \sigma_a^2 + (X\sigma_b)^2 + 2X\mathrm{Cov}(a,b) = \sigma_a^2 + (X\sigma_b)^2 - 2X\bar{X}\sigma_b^2 \quad (2)$$

where σ is the standard deviation, Cov(a,b) is the covariance of a (intercept) and b (slope), X = 1/T(K), $\bar{X}$ is the mean of X and Y = logD.

The comparison of D(Sm) data in Figure 7 shows that our data cannot be reconciled with those of Van Orman et al. (2002a) unless ΔV^+ is significantly larger than their suggested value of 10 cm^3/mol. However, we feel that a value of ΔV^+ of ~ 15 cm^3/mol that is required to bring our data set to be barely in agreement with those of Van Orman et al. (2002a) is rather too large to be correct, in view of the measured values of ΔV^+ of the divalent cations Mg, Fe, and Mn in garnet (Chakraborty and Ganguly, 1992). Thus, at this stage the discrepancy be-

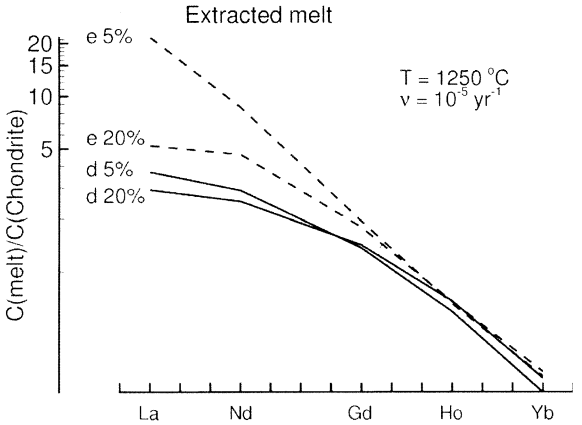

Fig. 10. Chondrite normalized concentration of REE in the extracted melt for 5 and 20% partial melting at 40 kb, 1250°C for normalized melting rate (ν) of 10^{-5} yr^{-1}. The letter symbol **e** stands for the equilibrium melt composition, whereas **d** stands for the melting composition for a melting rate (normalized to initial volume of crystal) of 10^{-5}/yr.

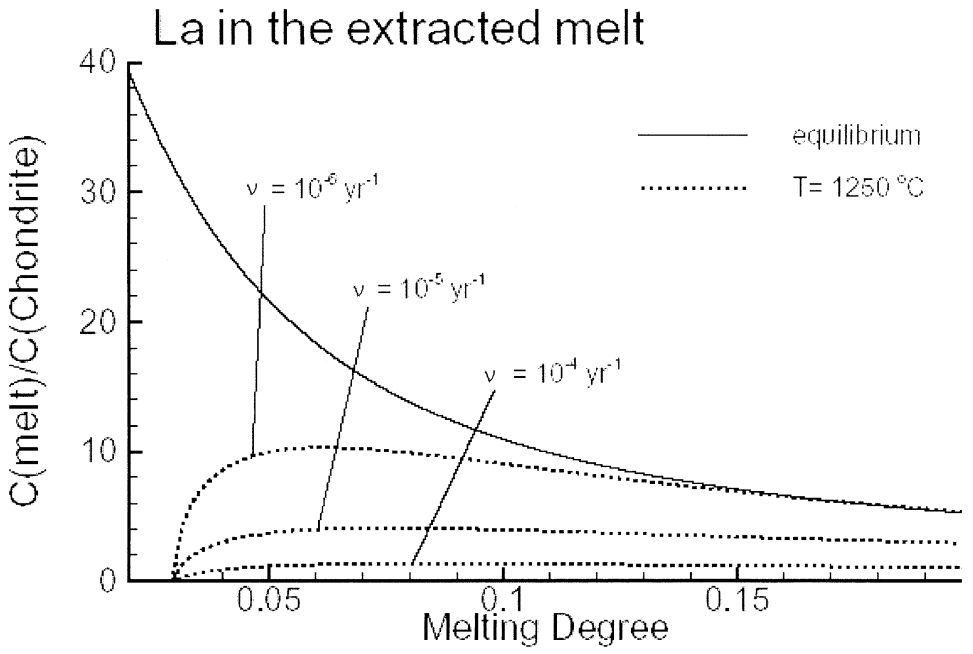

Fig. 11. Chondrite normalized concentration of La in the melt as a function of the partial melt fraction (melting degree) and normalized melting rate (ν) at 40 kb, 1250°C (dotted lines). The equilibrium melt composition is shown as a solid line.

tween the data of Van Orman et al. (2002a) and ours remain unresolved. We would test these data sets against constraints from natural data in a later section.

On the basis of the diffusion data that were derived from the SIMS analyses, and the above analysis and assumptions, we can express D(Sm) in garnet as a function of temperature, pressure, fO_2 and the Mg content as

$$\log D(P) \approx -4.20 - \left(\frac{13285 + 52P(kb)}{T}\right) + \frac{1}{6}\Delta\log fO_2 - 1.79(X_{Mg} - 0.22) \quad (3)$$

where $\Delta\log fO_2 = \log fO_2(\text{sample}) - \log fO_2(\text{WI buffer})$.

6. ARRHENIAN RELATION FOR DIFFERENT REE IN ALMANDINE GARNET

We do not have adequate data to derive the Arrhenian relation for the tracer diffusion kinetics of the rare earths in garnet other than Sm and Nd. Since the diffusion coefficients of the different rare earths differ very little (Fig. 5), the Arrhenian relation for any one of them can be used for the others without introducing significant errors. However, as discussed below, once an Arrhenian relation is defined for one of the rare earths, it is possible to provide theoretical constraints to the values of the preexponential factor, D_o, for the others for which we have limited diffusion data.

For diffusion by a vacancy mechanism, D_o can be expressed as (e.g., Mrowec, 1980)

$$D_0 \propto \nu e^{\Delta S/R} \quad (4)$$

where ΔS is the total entropy change (due to both vacancy formation and migration) and ν is a frequency factor which, in the first approximation, is equal to the frequency of vibration of the diffusing atom in the lattice site (Debye frequency). Assuming a spring model for the vibrational frequency,

$$\nu = \frac{k}{\sqrt{m}} \quad (5)$$

where k is the elastic constant and m is the mass of the diffusing atom.

ΔS can be expressed as (Zenner, 1952)

$$\Delta S \approx \beta\frac{Q}{T_m} \quad (6)$$

where T_m is the melting temperature and the parameter β is given by

$$\beta = -\frac{\partial(u/u_0)}{\partial(T/T_m)} \quad (7)$$

(Wert and Zenner, 1950), where u and u_o are the shear modulii at temperature T and 0 K, respectively. Combining Eqn. 4 through 7, we obtain for the ratio of D_o values of two REE, for example Sm (for which the Arrhenian parameters are known from Eqn. 1b) and Yb, in garnet as

$$\frac{D_0(Sm)}{D_0(Yb)} = \left(\frac{m(Yb)}{m(Sm)}\right)^{\frac{1}{2}} \exp\left(\frac{1}{R}\frac{\partial(u/u_0)}{\partial T}(-Q(Sm) + Q(Yb)\right) \quad (8)$$

A measured value of D(Yb) yields another independent relation between D_o(Yb) and Q(Yb) according to the Arrhenian expression, $D = D_o\exp(-Q/RT)$. Thus, using D_o(Sm) and Q(Sm) from

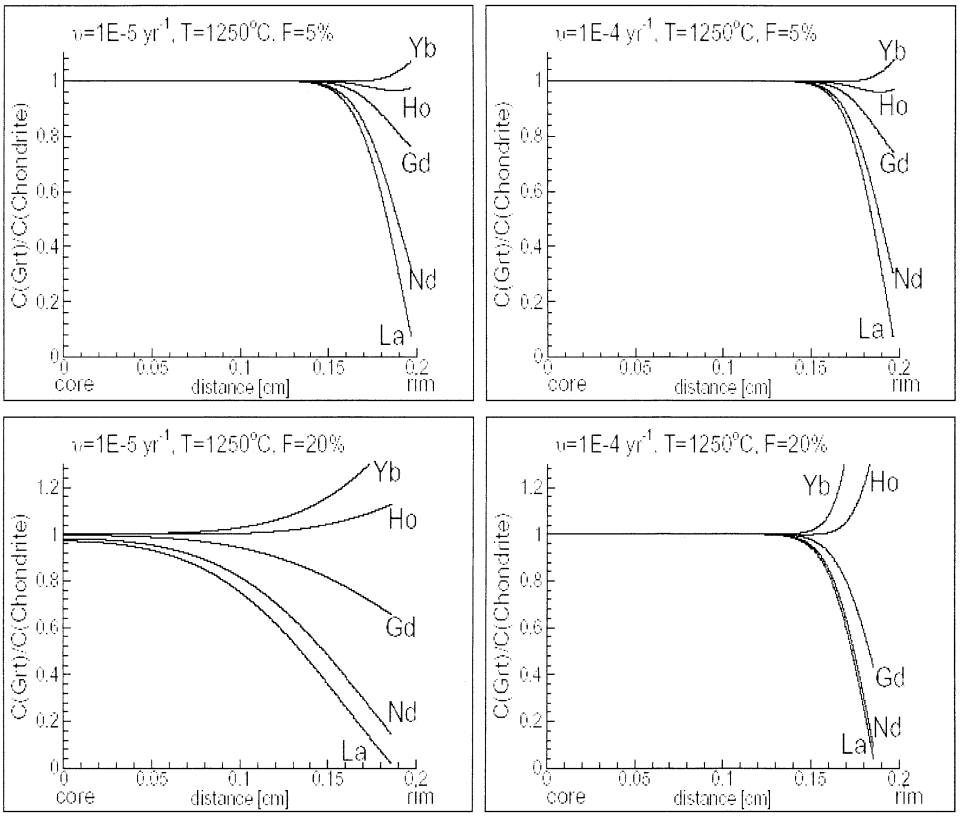

Fig. 12. Development of compositional zoning in garnet subjected to 5 and 20% partial melting at 40 kb, 1250°C at normalized melting rates of 10^{-4} and 10^{-5} per year. The garnet crystal is assumed to be spherical with an initial radius of 2 mm. A melting rate of 10^{-4} and 10^{-5} per year seems to be needed for the observed $^{226}Ra/^{230}Th$ disequilibrium in volcanic rocks.

Eqn. 1b, we can solve for both $D_o(Yb)$ and Q(Yb) if $\partial(u/u_o)/\partial T$ is known.

Van Orman et al. (2001) deduced a value of $\partial(u/u_o)/\partial T = -1.3 \times 10^{-4}\ K^{-1}$ for diopside. If we assume this value to be also valid for garnet, then using Eqn. 8 and the measured values of D(Yb) and D(Gd) at 1 bar, 1300°C (Table 1), we obtain $D_o(Yb) = 5.6 \times 10^{-5}\ cm^2/s$, Q(Yb) = 250830 J/mol, and similarly $D_o(Gd) = 6.0 \times 10^{-5}\ cm^2/s$ and Q(Gd) = 252738 J/mol for almandine garnet. These estimates of Arrhenian parameters are not very sensitive to the assumption of the value of the temperature dependence of u/u_o. For example, increasing it by a factor of 2 yields $D_o(Gd) = 6.0 \times 10^{-5}\ cm^2/s$ and Q(Gd) = 252836 J/mol. Thus, we use the Arrhenian parameters of Yb and Gd, estimated on the basis of the diopside value of $\partial(u/u_o)/\partial T$, along with those of Sm (Eqn. 2) to derive an expression of the tracer diffusion coefficient of REE in almandine ($Alm_{75}Pyr_{23}$) at 1 bar and fO_2 corresponding to that of WI buffer as a linear function of ionic radius, r. The values of ionic radii are taken from Shannon and Prewitt (1969). The expression is

$$D \approx (-0.11 + 5.8r)10^{-5}\exp[(-226264 - 25044r)/RT], \quad (9)$$

where r is in Å. Incorporating the fO_2, pressure, and compositional dependence of D from Eqn. 3, we finally derive a general expression for the tracer diffusion coefficient of REE in garnet as

$$\log D(REE) \approx -5 + \log(-0.11 + 5.8r) - \frac{1}{T}\left(\frac{98248 + (10875)r}{R} + 52P\right) + \frac{1}{6}\Delta\log fO_2 - 1.79(X_{Mg} - 0.22) \quad (10)$$

where P is in kb and $\Delta\log fO_2 = \log fO_2$ (sample) $- \log fO_2$ (WI buffer). The diffusion coefficients of Nd, Gd, and Yb in a pyrope garnet ($X_{Mg} = 0.50$) calculated from the above equation agree very well with those shown in Figure 5.

7. APPLICATIONS OF THE REE DIFFUSION DATA IN GARNET

The REE diffusion data in garnet have a wide range of applications to both magmatic and metamorphic processes. Ganguly et al. (1998) discussed the applications of the Sm-Nd diffusion data to the problem of closure temperature of the Sm-Nd decay system in garnet as a function of grain size and cooling rate, and also developed a method, using these diffusion data, to retrieve both cooling rate and closure temperature from the extent of resetting of the Sm-Nd age of garnet during cooling. Here we revisit the problem of closure temperature briefly, and then show applications of the REE diffusion data in garnet to the problem of disequilib-

rium partial melting process, and modeling of REE zoning in garnet from kimberlite.

7.1. Closure Temperature of Sm-Nd Decay System in Garnet

Mezger et al. (1992) determined the Sm-Nd age of garnet of 1 to 5 mm in apparent diameter in thin section, and composition $Alm_{77}Prp_{22}Grs_4Sps_4$, from the Pikwitonei granulite domain of the Superior province, Canada. Using two-feldspar thermometry, they estimated a peak metamorphic temperature of ~ 750°C for these granulites. The Sm-Nd age of garnet is ~ 30 Myr younger than the peak metamorphic age of ~ 2640 Ma, as determined by U-Pb ages of zircon and garnet. On the basis of a cooling curve or temperature-time (T-t) relation determined from the age of three decay systems, spanning a range of 2430 to 2640 Ma, vs. their respective closure temperatures, T_c, Mezger et al. (1992) estimated a $T_c = 650 \pm 30$°C for the Sm-Nd decay system in these garnets and a cooling rate of ~ 2°C/Myr.

We have calculated the T_c of the garnets studied by Mezger et al. (1992) using their estimated T_o and cooling rate and a grain diameter of 3 mm, which is at the midpoint in the range of grain sizes (1 to 5 mm) used by them. The T_c was calculated from the extension of Dodson formulation (Dodson, 1973) by Ganguly and Tirone (1999) that makes it suitable for slowly diffusing systems. The results of calculation using the Sm diffusion data of Van Orman (2002a) and Ganguly et al. (1998), as slightly modified in this study, are illustrated in Figure 8. There is very good agreement between the T_c estimated by Mezger et al. (1992) and that calculated from the diffusion data of this study, whereas T_c calculated from the best fit to the diffusion data of Van Orman et al. (2002a) for Mg-rich garnet is essentially the same as the peak temperature. Correction for the compositional effect according to our data only slightly reduces T_c (Van Orman), which is shown as a dashed curve in Figure 8. A more detailed calculation of T_c of Sm-Nd decay system in almandine garnet as a function of cooling rate and grain size is given by Ganguly et al. (1998). In the latter, ΔV^+ was assumed to be 6 cm^3/mol, which is the measured value for Mn^{2+}—the largest cation for which well constrained data are available for diffusion in garnet. The smaller value of ΔV^+ yielded slightly lower T_c than that calculated in this work, for example, 660°C for cooling rate of 2°C/Myr, using the parameters shown in Figure 8.

7.2. REE Pattern of Partial Melt and Residual Garnet

The rare earth pattern in magmas produced from the partial melting of a mantle peridotite depends on the equilibrium distribution coefficient of these elements between the solids and the melt, their diffusivities in the solid, and the rates of melting and melt extraction. Since garnet and clinopyroxene are the major carriers of REE in mantle peridotites, it is the diffusion properties and solid-melt distribution coefficients of these phases that are of primary importance in the modeling of the evolution of REE pattern during partial melting process. The importance of diffusion in minerals in disequilibrium melting has been recognized by several authors who developed various models to incorporate the diffusion effect in the melting process (e.g., Navon and Stolper, 1987; Iwamori, 1992; Spiegelmann and Kenyon, 1992; Qin, 1992; Iwamori, 1993; Korenaga and Kelemen, 1997; Van Orman et al. 2002b). Here we base our analysis of the problem using Qin's approach and consider only the effect of diffusion in garnet, although a full analysis of the problem requires consideration of the effect of diffusion in clinopyroxene as well. This exercise is meant to explore, using our diffusion data, the potential disequilibrium effects on the REE pattern of melts, and the effect of disequilibrium melting on the compositional zoning in residual garnet. The latter analysis has not been done in any earlier study using any diffusion data.

Van Orman et al. (2001) and Tirone (2002) determined the REE diffusion kinetics in clinopyroxene, but the diffusion coefficients determined by Tirone (2002) are significantly larger and comparable to those in garnet, as determined in this study. We thus postpone consideration of the REE diffusion kinetics in clinopyroxene until the difference between the two data sets are sorted out. Our conclusions about the effect of dynamic melting would hold if clinopyroxene has similar REE diffusivities as garnet in our study. On the other hand, the disequilibrium effect of dynamic melting would be even stronger than we calculate if the tracer diffusivities of REE in clinopyroxene are significantly smaller than those in garnet.

The general structure of Qin's (1992) model is as follows. A trace element is transferred from a solid to a melt by partial melting on the crystal surface at a rate υ_m, and by diffusion. There are three reservoirs of the trace elements: the solid, the residual melt that remains within the pore spaces of the solid, and the segregated melt that forms by extraction of the residual melt at a rate υ_e. The crystal is assumed to have a spherical geometry, which is the appropriate average geometry for garnet. The concentration of a species in the solid (C_s) of radius r with an initial uniform composition C_o is given by the solution of the diffusion equation in spherical coordinates

$$\frac{\partial C_s}{\partial t} = D\left(\frac{\partial^2 C_s}{\partial r^2} + \frac{2}{r}\frac{\partial C_s}{\partial r}\right) \quad 0 \le r \le R(t) \tag{11}$$

subject to the condition that the concentration at the boundary of the crystal ($r = R(t)$), C_b, is always in equilibrium with the residual melt. Thus, if K is the equilibrium partition coefficient between the mineral and the melt, then $C_b = KC_m(t)$. Qin (1992) assumed a constant melt fraction in the solid matrix such that when the melt fraction exceeds this value, the extra melt is extracted immediately to the segregated pool. Following Qin (1992), one can compute the concentration of an element in the residual and the segregated melt as a function of the grain size of the solid, degree of partial melting, and normalized melting rate, υ, which is given by υ_m/V_o, where υ_m is the volume of the solid transferred into the melt per unit time and V_o is the original volume of the solid grain.

Qin (1992) defined a nonequilibrium parameter, N_e, as the dimensionless ratio $\upsilon R_o^2/D$, where R_o is the initial radius of the crystal. Larger the value of N_e, greater is the departure from the equilibrium melting behavior. When N_e is close to zero, we have effectively equilibrium melting behavior. However, even for large N_e, effectively equilibrium melting prevails when the extent of partial melting exceeds a critical value that depends on the partition coefficient. The role of partition coefficient can

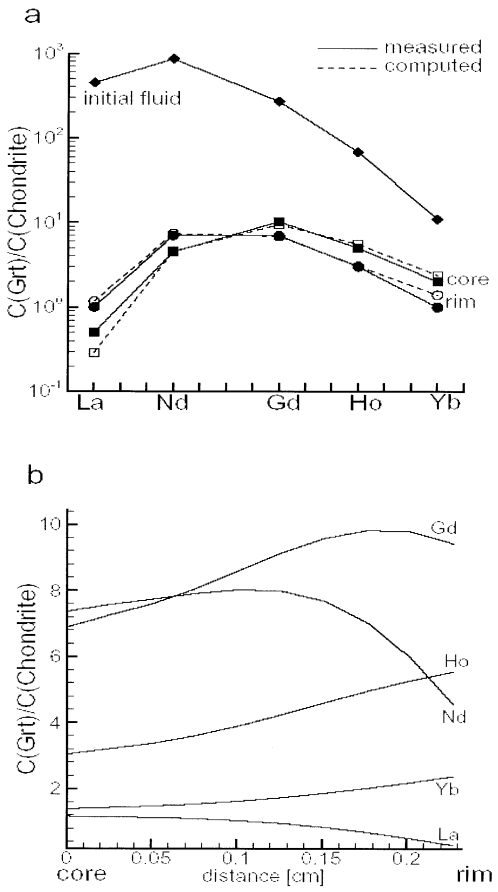

Fig. 13. (a) Chondrite normalized REE compositions of core and rim of a garnet crystal, as measured (filled symbols) by Hickmott (1989), and simulation (open symbols) of these compositions after contact with a melt of an assumed initial composition for 32,000 yr, at 40 kb, 1300°C, and fO_2 corresponding to that of QFM buffer. (b) Compositional zoning of different REE in the same garnet.

be appreciated by noting that regardless of the value of N_e, the concentration of a trace element in the melt would be the same as that in the equilibrium melting behavior when the partition coefficient, K, is unity. Qin (1992) showed that for K <0.01, effectively complete equilibrium and complete disequilibrium melt behavior would hold for $N_e \leq 0.1$ and $N_e \geq 10$, respectively, for geologically reasonable mass fraction of the partial melt, which is ≤0.20. According to McKenzie (1991), K is 0.01 for La, 0.087 for Nd, 0.498 for Gd, 1.53 for Ho, and 4.03 for Yb.

For mantle melting, Qin (1992) estimated an average value of υ of $\sim 10^{-7}$/yr. However, he argued that a value of 10^{-4} to 10^{-5}/yr is needed to account for the observed $^{226}Ra/^{230}Th$ disequilibrium in volcanic rocks (Condomines et al., 1988). Using the Sm diffusion data as determined in this study (Eqn. 3), we first illustrate the variation of N_e as a function of temperature at P = 30 kb, $fO_2 \sim$ QFM buffer, υ of 10^{-4}, 10^{-5} and 10^{-6}/yr, and several values of initial grain radius, R_o (Fig. 9). The transition from partial to effectively complete disequilibrium for K = 0.01 is shown by a horizontal line.

For dry melting of peridotite, which requires adiabatic upwelling, the solidus temperature is at least 1400°C (Green et al., 2001; Presnall et al., 2002). It is evident from Figure 9 that for initial grain size smaller than 2 mm radius and dry melting, the REE concentration in melt for dry melting would be very close to that for the limiting case of equilibrium melting, even for the fastest inferred melting rate of 10^{-4}/yr. For melting under hydrous (Kushiro et al., 1968) or CO_2 dominated conditions (Presnall et al., 2002), the solidus temperature is, however, much lower at pressures within the garnet stability field, and could be as low as ~1050°C if H_2O is the only volatile species. Significant departure of REE pattern in melt from equilibrium melting behavior would be expected under this condition. The hypothesis that melting beneath ridges has been taking place in the presence of water (Asimow and Langmuir, 2003) and that plumes such as in the Hawaiian region carry a significant CO_2 component (Sen, 1983) implies much lower solidus temperature in these regions than that under dry condition. Melting in the mantle wedge above a subducting slab has also been taking place as a consequence of the depression of solidus temperature by water given off by the dehydration of minerals in the slab (e.g., Bose and Ganguly, 1995).

Using our REE diffusion data for garnet, we have performed a series of calculations to explore the evolution of melt and mineral compositions under both equilibrium and dynamic melting conditions. Figure 10 shows the chondrite normalized REE pattern of melt for 5 and 20% partial melting at 40 kb, 1250°C, and melting rate of 10^{-5} yr^{-1}. The equilibrium concentrations of REE in melt were calculated according to the relations (Qin, 1992)

$$\frac{C_i^m}{C_i^0} = \frac{1}{(1-F)K_i + f} \quad \text{for } f \leq \phi \qquad (12a)$$

and

$$\frac{C_i^m}{C_i^0} = G\left(\frac{1-f}{1-\phi}\right)^{G(1-\varphi)(1-K_i)} \quad \text{for } f \geq \phi \qquad (12b)$$

where ϕ is the threshold value of the residual melt before extraction, $G = 1/[\phi + D_i(1-\phi)]$, C_i^o is the initial concentration of i in the mineral, and f is the melt fraction. It is evident from Figure 10 that for $f \leq 0.05$ (5% melting), $\upsilon \geq 10^{-5}$ yr^{-1}, the concentrations of light REE in the melt produced by near-solidus melting in the presence of a H_2O rich vapor phase could be significantly lower than their equilibrium concentrations, and the overall REE pattern of the melt could mimic that for a melt derived from a much larger extent of equilibrium partial melting (compare, for example the pattern of 5% dynamic melting with that of 20% equilibrium melting). The concentration of La in the melt as a function of the normalized melting rate and degree of partial melting or melt fraction at 40 kb, 1250°C, and R_o of 2 mm, is illustrated in Figure 11. It shows that La concentration in the melt should be significantly lower than that under equilibrium conditions at small degrees of partial melting in the presence of a H_2O rich vapor phase that would cause partial melting at 1250°C or even at lower temperature.

We have also calculated the concentration profiles (Fig. 12) of selected REE from La to Yb in garnet of 2 mm radius at the above P, T condition, and $\upsilon = 10^{-4}$ and 10^{-5} yr^{-1}. The garnets are found to be strongly zoned in the rare earth elements that

fractionate significantly between the mineral and the melt. The calculations show that the compositional zoning in garnet (and in other residual solids) preserve important records of the rate and degree of partial melting. However, measurement of such compositional zoning is scarce. The difference in the zoning profiles of the different REE, all of which have similar diffusivities, is a consequence of the difference in their mineral-melt partitioning values, which produce a much larger compositional gradient for the light REE in garnet relative to those for the heavy REE.

7.3. REE Zoning in a Garnet From Lherzolite Xenolith in a Kimberlite

Hickmott (1989) determined the REE concentrations in the cores and rims of two pyrope garnet crystals, one from a sheared and the other from a granular garnet lherzolite from the Archean Kaapval craton, S. Africa. The results for the garnet in the granular lherzolite suite that are illustrated in Figure 13 show a small but distinct difference between the concentration of the REE in the core and the rim. We have modeled these core to rim variations of the REE in the garnet in terms of a few different processes to understand how these REE compositional variations might have been produced. We considered a dynamic melting process in which the melting rate, temperature, and composition of the initial melt were allowed to vary.

A very good fit to the measured REE data in the garnet was obtained by considering a single melting episode in which the garnet underwent a partial melting after coming in contact with another melt derived from a different source with the following initial composition: La = 450 ppm, Nd = 860 ppm, Gd = 270 ppm, Ho = 78 ppm, and Yb = 11 ppm. The initial REE concentration of the garnet was assumed to be homogeneous and chondritic. The other parameters are: T = 1300°C, P = 40 Kbar, υ = 7.8 x 10 − 6 yr^{-1}, and t = 32,000 yr and initial crystal radius of 2.5 mm. The assumed initial melt composition and the comparison between the simulated and measured core and rim compositions of garnet are illustrated in Figure 13a. The calculated zoning profiles of the REE in garnet are illustrated in Figure 13b. These results suggest that if chemical interaction with an externally derived magma were responsible for the observed compositional zoning in garnet, then the residence time of the xenolith in the magma before eruption was most likely ~ 32,000 yr. Furthermore, our calculations demonstrate how the REE zoning in mantle xenoliths can be used to develop insights into the mantle processes.

Acknowledgments—This research was primarily supported by US National Science Foundation grant No. EAR 9805232 and a NASA grant No. COS03-0030-0025. JG gratefully acknowledges the support from Alexander von Humboldt Forschungspreis that made the collaboration with the German institutions possible, and the hospitality of Profs. Dave Rubie and Sumit Chakraborty. The paper has greatly benefited from the reviews of Dr. Danile Cherniak and two anonymous reviewers and the editorial comments and criticisms of Dr. Rick Ryerson.

REFERENCES

Asimow P. D. and Langmuir C. H. (2003) The importance of water to oceanic mantle melting regimes. *Nature* **421,** 815–820.

Bose K. and Ganguly J. (1995) Experimental and theoretical studies of the stabilities of talc, antigorite and phase A at high pressures with applications to subduction processes. *Earth Planet. Sci. Lett.* **136,** 109–122.

Chakraborty S. and Ganguly J. (1992) Cation diffusion in aluminosilicate garnets: experimental determination in spessartine-almandine diffusion couples, evaluation of effective binary diffusion coefficients and applications. *Contrib. Mineral. Petrol.* **111,** 74–86.

Condomines M., Hémond C., and Allègre C. J. (1988) U-Th-Ra radioactive disequilibria and magmatic processes. *Earth Planet. Sci. Lett.* **90,** 243–262.

Crank J. (1975) Mathematics of diffusion. Oxford.

Dodson M. J. (1973) Closure temperatures in cooling geochronological and petrological systems. *Contrib. Mineral. Petrol.* **40,** 259–274.

Ducea M. N., Ganguly J., Rosenberg E. J., Patchett P. J., Cheng W., and Isachsen C. (2003) Sm-Nd dating of spatially controlled domains of garnet single crystals: a new method of high-temperature thermochronology. *Earth Planet. Sci. Lett.* **213,** 31–42.

Ganguly J. and Tirone M. (1999) Diffusion closure temperature and age of a mineral with arbitrary extent of diffusion: theoretical formulation and applications. *Earth Planet. Sci. Lett.* **170,** 131–140.

Ganguly J., Tirone M., and Hervig R. L. (1998a) Diffusion kinetics of samarium and neodymium in garnet and a method of determining cooling rates of rocks. *Science* **281,** 805–807.

Green D. H., Fallon T. J., Eggins S. M., and Yaxley G. M. (2001) Primary magmas and mantle temperatures. *Eur. J. Mineral.* **33,** 437–451.

Hickmott D. D. (1989) Rare earth element zoning in pyrope-rich garnet from mantle xenoliths. *Annual Report of the Director of the Geophysical Laboratory 1988–1989,* 6–10.

Hsu L. C. and Burnham C. W. (1969) Phase relations in the system $Fe_3Al_2Si_3O_{12}$- $Mg_3Al_2Si_3O_{12}$-H_2O at 2.0 Kilobars *Bull. Geol. Soc. America* **80,** 2393–2408.

Iwamori H. (1992) Melt-solid flow with diffusion-controlled chemical reaction. *Geoph. Res. Lett.* **19,** 309–312.

Iwamori H. (1993) Dynamic disequilibrium melting model with porous flow and diffusion-controlled chemical equilibration. *Earth Planet. Sci. Lett.* **114,** 301–313.

Jaoul O., Sautter V. and Abel F. (1991) Nuclear microanalysis: a powerful tool for measuring low atomic diffusivity with mineralogical applications. In *Diffusion, Atomic Ordering and Mass Transport. Advance in Physical Geochemistry* (ed. J. Ganguly), pp. 198–220, Springer-Verlag.

Korenaga J. and Kelemen P. B. (1997) Melt migration through the oceanic lower crust: a constraint from melt percolation modeling with finite solid diffusion. *Earth Planet. Sci. Lett.* **156,** 1–11.

Kotai E. (1994) Computational methods for analysis and simulation of RBS and ERDA spectra. *Nucl. Instr. Meth. B* **85,** 588–596.

Kushiro I., Syono Y., and Akimoto S. (1968) Melting of a peridotite nodule at high pressures and high water pressure. *J. Geophys. Res.* **73,** 6023–6029.

Lovering T. S. (1938) Heat conduction in dissimilar rocks and the use of thermal models. *Bull. Geol. Soc. Am.* **47,** 87–100.

McKenzie D. (1991) Partial melt distribution from inversion of Rare Earth Element concentrations. *J. Petrol.* **32,** 1021–1091.

Mezger K., Essene E. J., and Halliday A. N. (1992) Closure temperatures of the Sm-Nd system in metamorphic garnets. *Earth Planet. Sci. Lett.* **113,** 397–409.

Misener D. J. (1974) Cationic diffusion in olivine to 1400 °C and 35 kbar. In *Geochemical Transport and Kinetics,* Publication 634 (ed. A. W. Hoffmann et al.), pp. 117–129, Carnegie Institution of Washington.

Morioka M. and Nagasawa H. (1991) Ionic diffusion in olivine. In *Diffusion, Atomic Ordering and Mass Transport. Advance in Physical Geochemistry* (ed. J. Ganguly), pp. 176–197, Springer-Verlag.

Mrowec S. (1980) *Defects and Diffusion in Solids, an Introduction. Materials Science Monographs, 5.* Elsevier.

Nakamura A. and Schmalzried H. (1984) On the Fe2+ - Mg2+ - Interdiffusion in Olivine (II). *Ber. Bunsenges. Phys. Chem.* **88,** 140–145.

Navon O. and Stolper E. (1987) Geochemical consequences of melt percolation: the upper mantle as a chromatographic column. *J. Petrol.* **95,** 285–307.

Petry C., Chakraborty S., and Palme H. (2004) Experimental determination of Ni diffusion coefficients in olivine and their dependence on temperature, composition, oxygen fugacity and crystallographic orientation. *Geochim. Cosmochim. Acta* **68,** 4179–4188.

Presnall D. C., Gudfinnsson G. H., and Walter M. J. (2002) Generation of mid-ocean ridge basalts at pressure from 1 to 7 GPa. *Geochim. Cosmochim. Acta.* **66,** 2073–2090.

Qin Z. (1992) Disequilibrium partial melting model and its implications for trace element fractionations during mantle melting. *Earth Planet. Sci. Lett.* **112,** 75–90.

Ryerson F. J. and McKeegan K. D. (1994) Determination of oxygen self-diffusion in akermanite, anorthite, diopside and spinel; implications for oxygen isotopic anomalies and the thermal histories of Ca-Al-rich inclusions. *Geochim. Cosmochim. Acta* **58,** 3713–3734.

Sen G. (1983) A petrologic model for the constitution of the upper mantle and crust of the Koolau shield, Oahu, Hawaii and Hawaiian magmatism. *Earth Planet. Sci. Lett.* **62,** 215–228.

Shannon R. D. and Prewitt C. T. (1969) Effective ionic radii in oxides and fluorides. *Acta Cryst.* **B25,** 925–946.

Spiegelmann M. and Kenyon K. (1992) The requirements for chemical disequilibrium during magma migration. *Earth Planet. Sci. Lett.* **109,** 611–620.

Tirone M. (2002) *Diffusion of Rare Earth Elements in Garnet and Pyroxene: Experiment, Theory and Applications.* Ph.D. Thesis, University of Arizona.

Tirone M., Ganguly J., and Hervig R. L. (2000) Rare Earth Diffusion in Garnets: Tracer-Diffusion Experiments and Applications to the Interpretation of REE Patterns of Partial Melts and Residual Solids. *Eos Trans. AGU Fall Meet. Suppl.* **81** (*48*), Abstract V71B-35.

Van Orman J. A., Grove T. L., Shimizu N., and Graham D. L. (2001) Rare earth element diffusion in diopside: influence of temperature, pressure and ionic radius and an elastic model for diffusion in silicates. *Contrib. Mineral. Petrol.* **141,** 687–703.

Van Orman J. A., Grove T. L., Shimizu N., and Graham D. L. (2002a) Rare earth element diffusion in a natural pyrope single crystal at 2.8 GPa. *Contrib. Mineral. Petrol.* **142,** 416–424.

Van Orman J. A., Grove T. L., and Shimizu N. (2002b) Diffusive fractionation of trace elements during production and transport of melt in Earth's upper mantle. *Earth Planet. Sci. Lett.* **198,** 93–112.

Wert C. W. and Zenner C. (1950) Interstitial atomic diffusion. *J. Appl. Phys.* **21,** 1196–1175.

Zenner C. (1952) Theory of diffusion. In *Imperfections in Nearly Perfect Crystals* (ed. W. Shockleyet al.), pp. 289–314) Wiley.